JCI insight

RESEARCH ARTICLE

CD83 orchestrates immunity toward self and non-self in dendritic cells

Andreas B. Wild,[1] Lena Krzyzak,[1] Katrin Peckert,[1] Lena Stich,[1] Christine Kuhnt,[1] Alina Butterhof,[1] Christine Seitz,[1] Jochen Mattner,[2] Niklas Grüner,[2] Maximilian Gänsbauer,[2] Martin Purtak,[2] Didier Soulat,[2] Thomas H. Winkler,[3] Lars Nitschke,[3] Elisabeth Zinser,[1] and Alexander Steinkasserer[1]

[1]Department of Immune Modulation and [2]Institute of Microbiology – Clinical Microbiology, Immunology and Hygiene, Universitätsklinikum Erlangen and Friedrich-Alexander Universität Erlangen-Nürnberg, Erlangen, Germany. [3]Division of Genetics, Department of Biology, Friedrich-Alexander Universität Erlangen-Nürnberg, Erlangen, Germany.

Dendritic cells (DCs) are crucial to balance protective immunity and autoimmune inflammatory processes. Expression of CD83 is a well-established marker for mature DCs, although its physiological role is still not completely understood. Using a DC-specific CD83–conditional KO (CD83$^{\Delta DC}$) mouse, we provide new insights into the function of CD83 within this cell type. Interestingly, CD83-deficient DCs produced drastically increased IL-2 levels and displayed higher expression of the costimulatory molecules CD25 and OX40L, which causes superior induction of antigen-specific T cell responses and compromises Treg suppressive functions. This also directly translates into accelerated immune responses in vivo. Upon *Salmonella typhimurium* and *Listeria monocytogenes* infection, CD83$^{\Delta DC}$ mice cleared both pathogens more efficiently, and CD83-deficient DCs expressed increased IL-12 levels after bacterial encounter. Using the experimental autoimmune encephalomyelitis model, autoimmune inflammation was dramatically aggravated in CD83$^{\Delta DC}$ mice while resolution of inflammation was strongly reduced. This phenotype was associated with increased cell influx into the CNS accompanied by elevated Th17 cell numbers. Concomitantly, CD83$^{\Delta DC}$ mice had reduced Treg numbers in peripheral lymphoid organs. In summary, we show that CD83 ablation on DCs results in enhanced immune responses by dysregulating tolerance mechanisms and thereby impairing resolution of inflammation, which also demonstrates high clinical relevance.

Introduction

Dendritic cells (DCs) are crucial players in our immune system as they function as professional antigen-presenting cells (APCs) and connect innate and adaptive immune responses. Immature DCs are present in most tissues and are able to sense pathogens via conserved innate immune receptors, including Toll-like receptors (TLRs). Upon activation via these receptors, DCs mature and migrate to lymphoid organs, where they prime antigen-specific naive T cells and drive their differentiation into specific effector subsets (1).

These features render DCs as key players not only in physiological immune responses but also in autoimmunity. Presentation of self-antigens can lead to an activation and expansion of self-reactive T cells, provided that mature DCs express stimulatory receptors and cytokines (2). In contrast, immature DCs insufficiently costimulate T cells during antigen recognition and rather drive them into an anergic or a regulatory phenotype (3). Thus, the maturation state of DCs significantly affects whether self-reactive T cells are kept in check or get activated, leading to severe autoimmune responses.

One well-characterized marker for this phenotypic transition from immature to mature DCs is the expression of the CD83 molecule (4, 5). This member of the Ig superfamily is expressed primarily on activated leukocytes, including DCs and regulatory T cells (Tregs), as well as on thymic epithelial cells (TECs) (6–9). A soluble form of CD83 (sCD83), comprising the extracellular domain, was detected at low levels in sera of healthy individuals and in increased concentrations in patients with hematological malignancies (10–12), and reports suggested B cells as a major source of naturally occurring sCD83 (13). Several studies demonstrated profound immunomodulatory effects of sCD83 in different animal models of autoimmune diseases and transplantation (14–18).

Conflict of interest: The authors have declared that no conflict of interest exists.

Submitted: November 16, 2018
Accepted: September 4, 2019
Published: October 17, 2019.

Reference information: *JCI Insight*. 2019;4(20):e126246. https://doi.org/10.1172/jci.insight.126246.

Although sCD83 induces tolerogenic mechanisms (16, 19, 20), the precise function of membrane-bound CD83 (mCD83) on different cell types is less clear. However, it has been reported that by inhibiting membrane associated ring-CH-type finger 1–dependent (MARCH1-dependent) ubiquitination, CD83 stabilizes surface expression of MHC-II and CD86 on DCs and B cells (21, 22). The same mechanism, but MARCH8-dependent, causes decreased surface MHC-II levels on cortical TECs in $CD83^{-/-}$ mice (9, 23), resulting in defective positive selection and drastically reduced numbers of peripheral $CD4^+$ T cells (24). Additionally, our group revealed that expression of CD83 is essential for Treg homeostasis and stability (25).

However, the precise functional relevance of CD83 expression on APCs, such as DCs, is still not properly understood. On human DCs, CD83 expression was shown to correlate with enhanced T cell stimulatory capacity in vitro (26, 27). In contrast, deletion or overexpression of CD83 on murine APCs exhibited only a minor influence on their T cell–activating potential (28, 29). Because these data were conflicting and CD83 deficiency on APCs has been reported to influence mucosal homeostasis (30), we were interested in investigating the impact of CD83 deficiency on DCs in the context of intestinal infection/inflammation but also on neuroinflammation and the development of neurodegenerative autoimmunity.

Using the experimental autoimmune encephalitis (EAE) model, we show that specific deletion of CD83 on DCs led to an aggravated autoimmune neuroinflammation, which was hallmarked by increased influx of immune cells into the central nervous system (CNS) and a shift toward encephalitogenic Th17 responses. CD83-deficient DCs displayed higher levels of costimulatory CD25 and OX40L molecules on their surface and secreted more IL-2, which led to increased induction of antigen-specific T cell proliferation. Additionally, these DCs shaped a more inflammatory environment upon antigen-specific interaction with T cells. Interestingly, on the other hand, animals with DC-specific CD83 deletion showed improved bacterial clearance in acute intestinal infection models, suggesting a crucial regulatory function of CD83 for the balance between protective immunity and exacerbated autoimmune responses.

Results

Successful deletion of CD83 on DCs. To ablate CD83 expression in a cell-specific way, we used the previously reported Cre-*loxP* system for a conditional CD83 knockout (CD83 cKO) (29). Crossing $CD83^{fl/fl}$ mice with *Itgax*-Cre mice led to specific deletion of CD83 expression in $CD11c^+$ cells, especially in DCs ($CD83^{\Delta DC}$ mice) (Figure 1A). The successful KO of CD83 on DCs was proved at the mRNA and at the protein level using bone marrow–derived DCs (BMDCs). LPS-treated $CD83^{\Delta DC}$ BMDCs showed a complete abrogation of CD83 mRNA expression when compared with control mice (Figure 1B). On a protein level, $CD83^{fl/fl}$ BMDCs showed a strong increase in CD83 expression after LPS-induced maturation, whereas CD83 expression was lost in either unstimulated or LPS-matured $CD83^{\Delta DC}$-derived BMDCs, as demonstrated by Western blot analyses of whole-cell lysates (Figure 1C). Given the central role of DCs in the immune system, we evaluated the impact of DC-specific CD83 deletion on the cellular composition of the spleen of $CD83^{\Delta DC}$ mice. We detected no differences compared to control animals regarding the major cell subpopulations as well as naive, effector, and memory T cells (Supplemental Figure 1, A and B; supplemental material available online with this article; https://doi.org/10.1172/jci.insight.126246DS1).

Next, we assessed the effect of CD83 deletion on splenic DC subsets. First, we tested whether CD83 ablation altered the distribution of splenic DC subsets. However, neither the proportions of conventional DCs (cDC1, $CD11c^+CD8\alpha^+$; and cDC2, $CD11c^+CD11b^+$) nor plasmacytoid DCs (pDC, $B220^+SiglecH^+$) were changed in $CD83^{\Delta DC}$ mice (Supplemental Figure 1C). It was previously reported that splenic DCs display only low levels of CD83 but rapidly upregulate its surface display after in vitro stimulation with TLR ligands (4). Accordingly, we detected a small proportion of $CD83^+$ cells in both cDC subsets of the spleen, which correlated with high expression of MHC-II, while pDCs displayed only low levels of CD83 (Figure 1D and Supplemental Figure 1D). In contrast, cDCs from $CD83^{\Delta DC}$ mice expressed virtually no CD83. Furthermore, after DC maturation induced by the TLR-Ls CpG DNA and Pam_3CSK_4, CD83 expression was markedly induced in both cDC subsets derived from control animals but not from $CD83^{\Delta DC}$ mice (Figure 1D). Interestingly, expression of CD83 was not altered in pDCs when comparing $CD83^{fl/fl}$ and $CD83^{\Delta DC}$ mice (Supplemental Figure 1D). Therefore, we evaluated the deletion efficiency in all splenic DC subsets, using a Cre-reporter mouse strain. We detected nearly 100% reporter gene expression in both cDC1s and cDC2s, but a residual portion of pDCs showed no reporter gene expression (Supplemental Figure 1E), which may account for insufficient deletion in these cells.

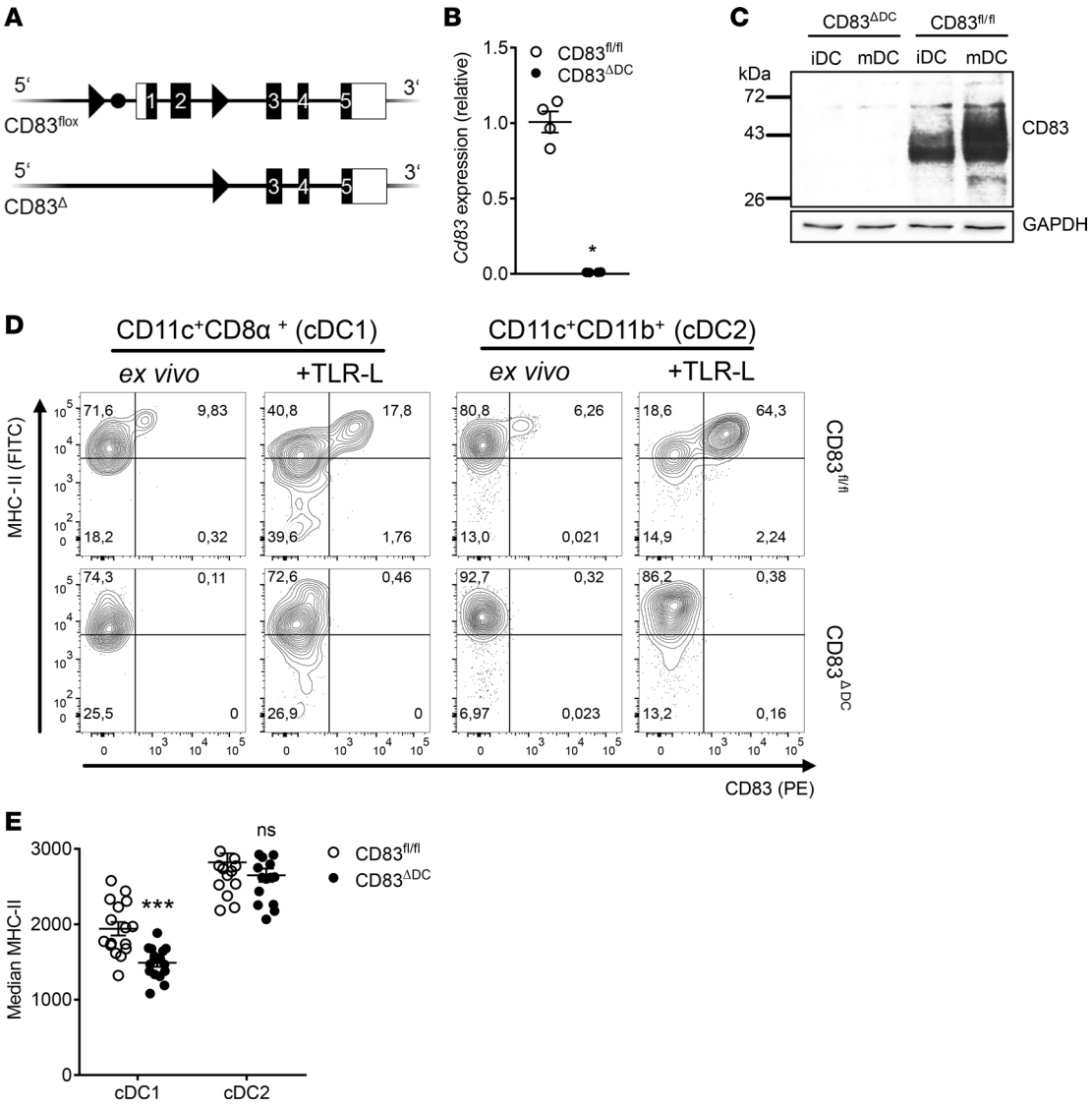

Figure 1. Successful deletion of CD83 on DCs. (**A**) Strategy used to generate DC-specific deletion of CD83 (CD83$^{\Delta DC}$). Mating of CD83$^{fl/fl}$ mice with *Itgax*-Cre mice led to deletion of *loxP*-flanked exons 1 and 2, resulting in ablation of CD83 expression, specifically in CD11c$^+$ DCs. (**B**) Assessment of KO efficiency on an mRNA level. BMDCs were matured with 0.1 μg/mL LPS for 16 hours, and expression levels of *Cd83* were determined via quantitative PCR (qPCR). Expression levels were normalized to CD83$^{fl/fl}$ BMDCs. (**C**) Assessment of knockout efficiency on a protein level. BMDCs were stimulated with 0.1 μg/mL LPS for 16 hours or left untreated, and CD83 expression was analyzed via Western blot of whole-cell lysates. GAPDH was used as a loading control. See full, uncut gels in online supplemental material. (**D**) Flow cytometric evaluation of CD83 deletion on splenic DC subsets. Total splenocytes were analyzed either ex vivo or after stimulation with 3.5 μg/mL CpG ODN2395 and 1 μg/mL Pam_3CSK_4 (TLR ligands, TLR-Ls) for 16 hours via flow cytometry. FACS data are representative of 5 mice. (**E**) Assessment of MHC-II surface expression on cDCs on splenic DC subsets. Data represent 4 independent experiments (n = 16). Data are represented as mean ± SEM. Statistical analysis was performed using Mann-Whitney U test. *P < 0.05; ***P < 0.001; ns, not significant. iDC, immature DC; mDC, mature DC.

CD83 was shown to stabilize the expression of MHC-II on APCs because of blockade of MARCH1-dependent ubiquitination and subsequent degradation (22). Thus, we examined whether DC-specific CD83 deletion would affect the surface expression of MHC-II molecules. Indeed, flow cytometric analyses of splenic DCs revealed that MHC-II expression was significantly reduced in cells derived from CD83$^{\Delta DC}$ mice (Figure 1E). The reduction of MHC-II expression was obvious on both cDC subsets, with the strongest effect on the cDC1 subset whereas cDC2s showed a less pronounced decrease. Additionally, CD83$^{\Delta DC}$-derived BMDCs displayed reduced MHC-II levels on their surface (Supplemental Figure 1E). Thus, using our cell type–specific knockout strategy, we successfully deleted CD83 in different DC subsets, which phenotypically led to diminished MHC-II cell surface expression.

CD83 deficiency confers an overactivated DC phenotype. The expression of peptide-loaded MHC-II on DCs is a prerequisite for initiation of antigen-dependent T cell responses, which further depend on sufficient

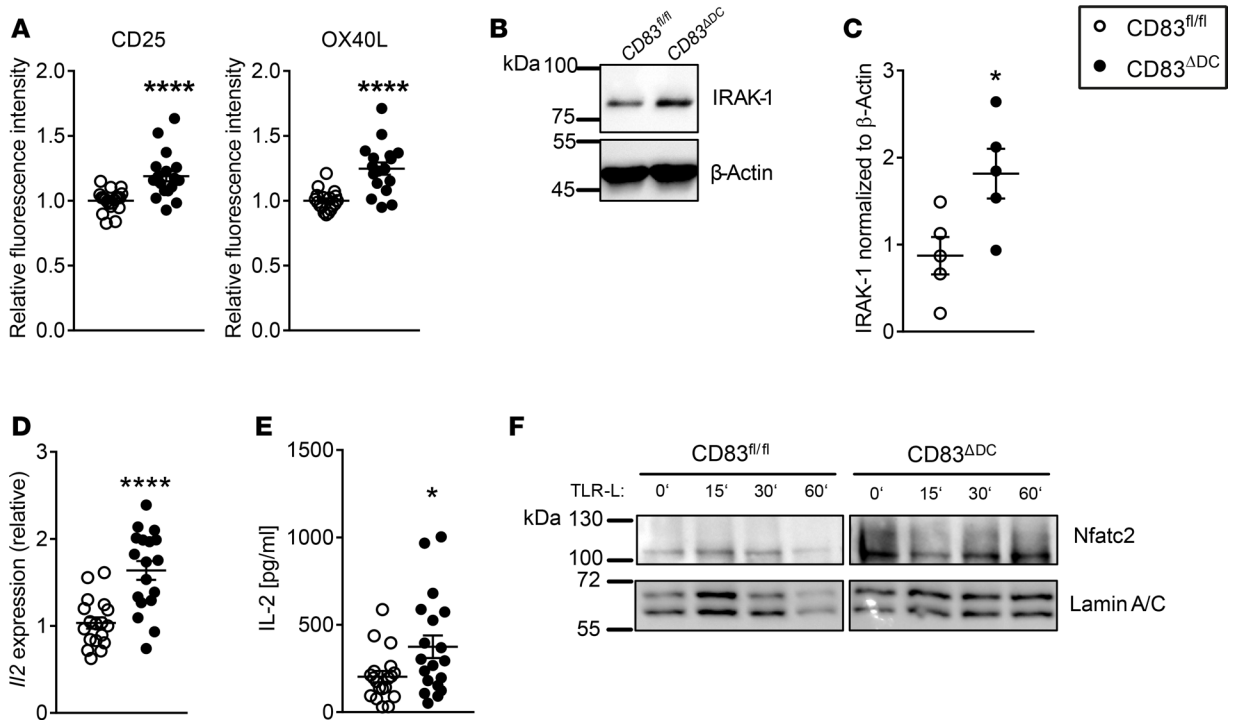

Figure 2. CD83 deficiency on DCs leads to enhanced costimulatory capacity. (**A**) Flow cytometry analysis of costimulatory surface markers. BMDCs were stimulated with 3.5 μg/mL CpG ODN2395 and 1 μg/mL Pam_3CSK_4 (TLR-Ls) for 16 hours, and expression of CD86, CD25, and OX40L was assessed on $CD11c^+MHC\text{-}II^{hi}$ mature DCs via flow cytometry. FACS data are pooled from 6 independent experiments, and the median fluorescence intensity was normalized to control animals (n = 20). (**B**) Western blot of cytoplasmic lysates of BMDCs unstimulated and probed against IRAK1. See full, uncut gels in online supplemental material. (**C**) Quantification of IRAK1 amounts in lysates from BMDCs (n = 5). (**D**) Expression of IL-2 after stimulation of DCs. BMDCs were stimulated with TLR-Ls for 6 hours, and expression of *Il2* mRNA was analyzed via qPCR (n = 18–20, pooled from 7 experiments). (**E**) Assessment of IL-2 secretion by BMDCs in response to TLR-Ls via ELISA. BMDCs were stimulated with TLR-Ls, and supernatant was collected after 16 hours (n = 19, pooled from 8 experiments). (**F**) Assessment of Nfatc2 in nuclear lysates from BMDCs. BMDCs were stimulated with TLR-Ls for indicated periods, harvested, and sequentially lysed (cytoplasm and nucleus). Nuclear fraction was separated with SDS-PAGE and transferred onto nitrocellulose membranes and probed with Nfatc2. Loading control for nuclear fraction was Lamin A/C. Blot is representative of 4 experiments. See full, uncut gels in online supplemental material. Data are represented as mean ± SEM (**A**, **C**, **D**, **E**). Statistical analysis was performed using Mann-Whitney U test. $^*P < 0.05$; $^{****}P < 0.0001$.

input from costimulatory receptors. Thus, we also examined the phenotype of CD83-deficient DCs with regard to costimulatory and coinhibitory molecules. However, neither the costimulatory molecules CD80 and CD40 nor the inhibitory receptors programmed cell death 1 ligand 1 (PD-L1) and PD-L2 revealed differences between CD83-deficient and control DCs after stimulation with TLR-Ls, although PD-L2 tended to be less expressed (Supplemental Figure 2, A and B). In contrast, we observed strikingly elevated surface levels of CD25 and OX40L on CD83-deficient BMDCs (Figure 2A and Supplemental Figure 2C), indicating a more activated phenotype. CD83 also stabilizes surface display of CD86, in a similar way as MHC-II (22), and accordingly we detected reduced levels of this molecule on CD83-deficient BMDCs after stimulation (Supplemental Figure 2D). Next, we examined whether this increased upregulation of costimulatory molecules could be attributed to altered TLR signaling in CD83-deficient DCs. Indeed, increased levels of interleukin-1 receptor-associated kinase 1 (IRAK1), which is a crucial component of the TLR signaling complex, were observed (Figure 2, B and C).

Because CD25 expression on DCs is crucial for IL-2 transpresentation to T cells as an early costimulatory signal (31), we assessed the IL-2 expression of BMDCs after activation. Interestingly, *Il2* mRNA levels were significantly elevated in CD83-deficient BMDCs after treatment with TLR-Ls (Figure 2D). Additionally, when we analyzed the supernatants of TLR-L–stimulated BMDCs after 24 hours, we detected highly increased amounts of IL-2 secreted by CD83-cKO BMDCs compared with controls (Figure 2E), which was even more striking when we took into account the interassay variability (Supplemental Figure 2E). In contrast to IL-2, we detected no differences in the expression of immunomodulatory molecules, such as TGF-β or indoleamine-2,3-dioxygenase 1, in CD83-deficient DCs after stimulation with TLR-Ls or LPS, respectively (Supplemental Figure 2F).

In T cells, IL-2 expression is controlled by the transcription factor Nfatc2, and this pathway is described in DCs as an important route for T cell stimulation (32). Thus, we were interested in whether Nfatc2 signaling in BDMCs was modified in CD83$^{\Delta DC}$ in comparison with control animals. Interestingly, when BMDCs were stimulated with TLR-Ls, we detected elevated Nfatc2 levels in the nuclear fraction of BMDCs derived from CD83-deficient mice (Figure 2F). Noteworthily, this effect was already apparent in unstimulated DCs, pointing to an overall more activated phenotype of CD83$^{\Delta DC}$-derived BMDCs, consistent with elevated expression of costimulatory molecules.

CD83-deficient DCs induce potent antigen-specific immune responses. On the one hand, CD83 deficiency on DCs resulted in degradation of MHC-II and CD86, which play crucial roles in initiating antigen-dependent T cell responses. On the other hand, we demonstrated that CD83-deficient DCs secreted more IL-2 and expressed higher levels of CD25 and OX40L. Both molecules have been reported to be involved in autoimmune disorders and autoreactive T cell activation (33, 34). Thus, we evaluated the capacity of CD83$^{\Delta DC}$ BMDCs to induce antigen-dependent T cell responses in a coculture system. To this end, BMDCs were activated with TLR-Ls, pulsed with the myelin oligodendrocyte glycoprotein peptide 35-55 (MOG_{35-55}), and subsequently cultivated with CD4$^+$ T cells from 2D2 mice carrying a transgenic MOG-specific T cell receptor.

Interestingly, cultivation with CD83-deficent DCs induced a pronounced proliferative response of 2D2 T cells as compared with controls (Figure 3, A and B). Most strikingly, the addition of a blocking antibody against OX40L to the cocultures reversed this positive effect on proliferation almost completely (Figure 3C). The antibody did not block the overall T cell response, as demonstrated by the nonsignificant change in proliferation for control DCs, but rather affected only CD83-deficient DCs, thus directly linking the altered surface phenotype to improved stimulatory capacity.

Besides the induction of T cell proliferation, DCs critically affect the type of T cell responses by shaping the cytokine milieu during the priming phase and differentiation (35). Thus, we next examined whether loss of CD83 on DCs would affect the microenvironment of DC–T cell interactions. To this end, we cocultivated TLR-L–activated and MOG_{35-55}-pulsed BMDCs with naive CD4$^+$ T cells, derived from 2D2 mice, and determined the cytokine levels within the supernatants of these cocultures. Notably, T cells cultivated with CD83-deficient BMDCs secreted considerably higher amounts of IL-17A, IL-6, and TNF-α, while IL-10 was drastically decreased (Figure 3D). Thus, deletion of CD83 on DCs led to an induction of a proinflammatory microenvironment during antigen-specific T cell stimulation. Because IL-6 and TNF-α are cytokines that critically contribute to Th17 polarization (36) and IL-17 secretion was indeed elevated, we reasoned that CD83-deficient DCs favor the development of antigen-specific Th17 responses.

Because we detected reduced amounts of the inhibitory cytokine IL-10, we next questioned whether the increased proliferative response of 2D2 T cells might rely on reduced expansion and/or induction of regulatory T cells in the cocultures. However, we detected no differences regarding Treg numbers after cocultivation (Supplemental Figure 4F). In contrast, when we tested the ability of Tregs to suppress antigen-specific T cell proliferation in the presence of BMDCs, we observed an impaired suppressive capacity in cocultures with CD83-deficient DCs (Figure 3E). These results indicate that CD83-deficient BMDCs (a) enhance antigen-specific T cell proliferation by providing stronger costimulatory signals and (b) modulate Treg-mediated suppression. Collectively, we demonstrated that CD83 deletion causes an overactivated DC phenotype, which is characterized by a highly increased potential to induce antigen-specific T cell proliferation and to shape a Th17-favoring cytokine milieu. Therefore, we were further interested in elucidating how this would affect immune responses to foreign and self-antigens.

Lack of CD83 expression on DCs enhances immune responses to acute infections. It has previously been reported that aberrant expression of MHC-II, as observed in *March1*$^{-/-}$ mice, disturbs DC homeostasis, reflected in severely impaired T cell stimulation and reduced IL-12 production (37, 38). In sharp contrast, we observed that CD83-deficient DCs, in which MHC-II ubiquitination and its destabilization are enhanced (22), exhibit improved T cell stimulatory capacity (Figure 3B). Thus, we scrutinized CD83$^{\Delta DC}$ DCs with regard to their ability to produce IL-12. Indeed, these DCs tend to secrete higher IL-12 levels upon TLR stimulation (Supplemental Figure 3, A and B). The IL-12 family cytokines IL-12 and IL-23 play important roles in the defense against intracellular bacteria, such as *Salmonella* (39, 40). Therefore, we analyzed the potential of CD83-deficient DCs to induce the expression of these cytokines upon bacterial encounter. To this end, we cultivated BMDCs with heat-killed *Salmonella typhimurium* (HKST) and assessed the expression of *Il12b*, *Il12a*, and *Il23a*, which respectively encode the IL-12p40, IL-12p35, and IL-23p19 subunits. BMDCs derived from CD83$^{\Delta DC}$ mice showed significantly increased *Il12b* expression levels after treatment

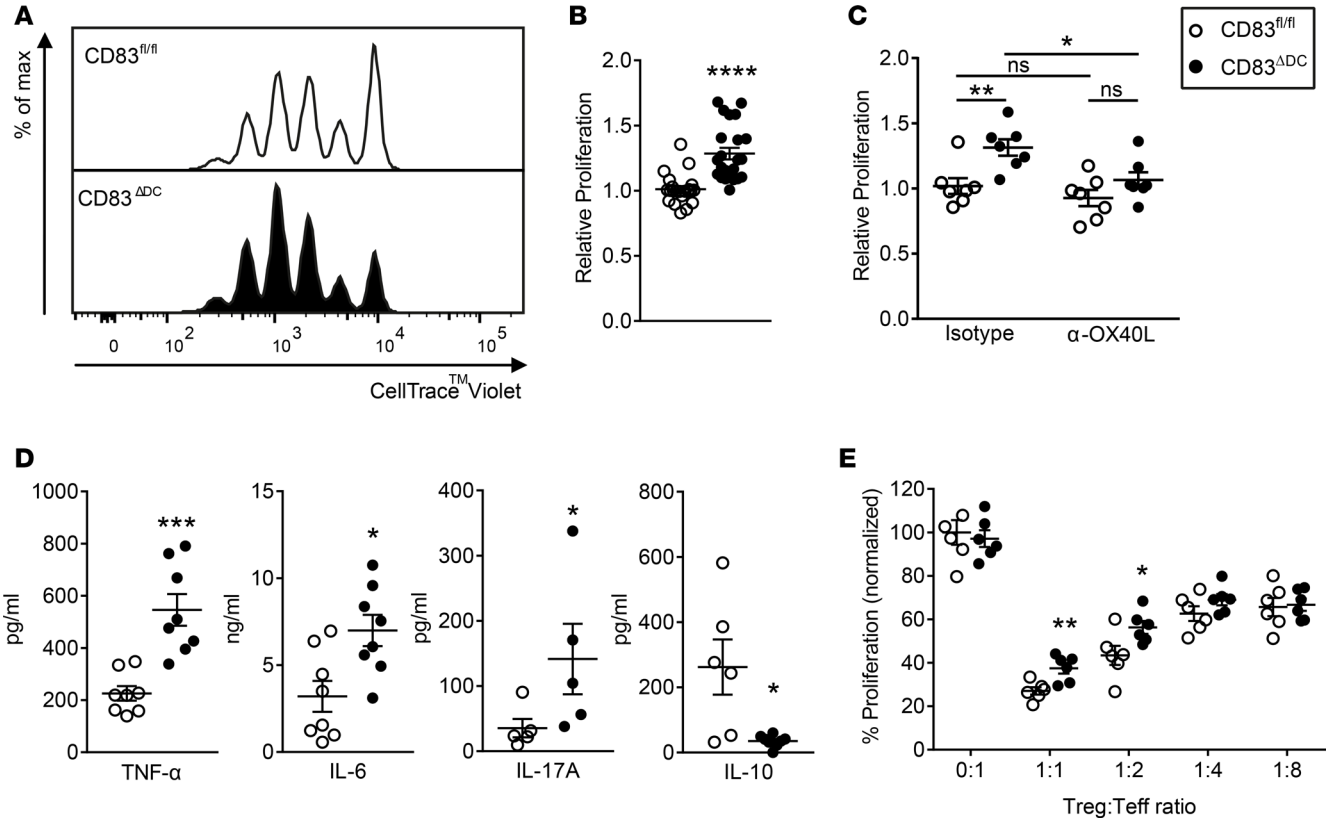

Figure 3. Ablation of CD83 boosts DC-mediated proinflammatory T cell responses. (**A** and **B**) Analysis of stimulatory capacity toward T cells. (**A**) BMDCs from CD83$^{\Delta DC}$ or control mice were activated with 3.5 μg/mL CpG ODN2395 and 1 μg/mL Pam_3CSK_4 (TLR-Ls) and pulsed with 2 μg/mL MOG_{35-55} for 3 hours and cocultivated with CellTrace Violet–labeled (CTV-labeled) 2D2-transgenic CD4$^+$ T cells. Proliferation was analyzed after 3 days of coculture via dye dilution on a flow cytometer. (**B**) Quantification of proliferative potential of T cells calculated from the ratio of median fluorescence of CTV. Data are pooled from 5 experiments (n = 14). (**C**) Proliferative response of 2D2 T cells to BMDCs in the presence of 10 μg/mL anti-OX40L (α-OX40L) or isotype-matched control antibody (n = 7, pooled from 2 independent experiments). (**D**) Assessment of cytokine secretion in BMDC–T cell cocultures. BMDCs were treated with TLR-Ls for 16 hours, and cytokine content in the supernatants were analyzed via cytometric bead array (n = 8 from 3 experiments). (**E**) Suppressive capacity of Tregs in cocultures. Tregs and effector T (T_{eff}) cells were cultured at different ratios with TLR-L–activated, MOG-pulsed BMDCs for 4 days (n = 6). Data are represented as mean ± SEM. Statistical analysis was performed using Mann-Whitney U test or 1-way ANOVA with Holm-Šídák correction for multiple comparisons (only for **C**). *P < 0.05; **P < 0.01; ***P < 0.001; ****P < 0.0001; ns, not significant.

with HKST. Moreover, *Il12a* and *IL23a* mRNA tended to be elevated in CD83-deficient DCs, indicating enhanced expression of both IL-12 and IL-23 (Figure 4A). We also tested the ability of BMDCs to secrete IL-12p40 in response to HKST and detected increased levels of this cytokine subunit in BMDC supernatants, thus corroborating our mRNA findings (Figure 4B).

Because IL-12 plays an important role in orchestrating the immune response to intracellular bacteria (41) and given that CD83-deficient BMDCs produce elevated levels of this cytokine in response to HKST in vitro, we investigated how CD83$^{\Delta DC}$ mice respond to bacterial infections. To this end, we infected mice with either *S. typhimurium* or *Listeria monocytogenes* and assessed the bacterial burden in specific organs. Because infection with *S. typhimurium* also leads to the development of colitis, we additionally determined the disease severity in these mice by histopathological analyses of the intestine. Interestingly, CD83$^{\Delta DC}$ mice (a) displayed lower levels of colitis and (b) exhibited a significantly lower bacterial burden in the liver and spleen, suggesting a reduced spreading of the pathogen to distal organs (Figure 4C). Similarly, infection with *L. monocytogenes* resulted in a significantly reduced bacterial spread to the liver in CD83$^{\Delta DC}$ mice, compared to controls, whereas the bacterial burden within the spleen of CD83$^{\Delta DC}$ mice revealed only a minor reduction (Figure 4D). Interestingly, we also detected increased expression of *Il12b*, *Il12a*, and *Il23a* in CD83-deficient DCs after treatment with heat-killed *Staphylococcus aureus* (Supplemental Figure 3C), suggesting a superior capacity to mount protective responses to bacteria. These data provide clear evidence that a DC-specific CD83 deficiency results in improved immune responses to acute bacterial infections.

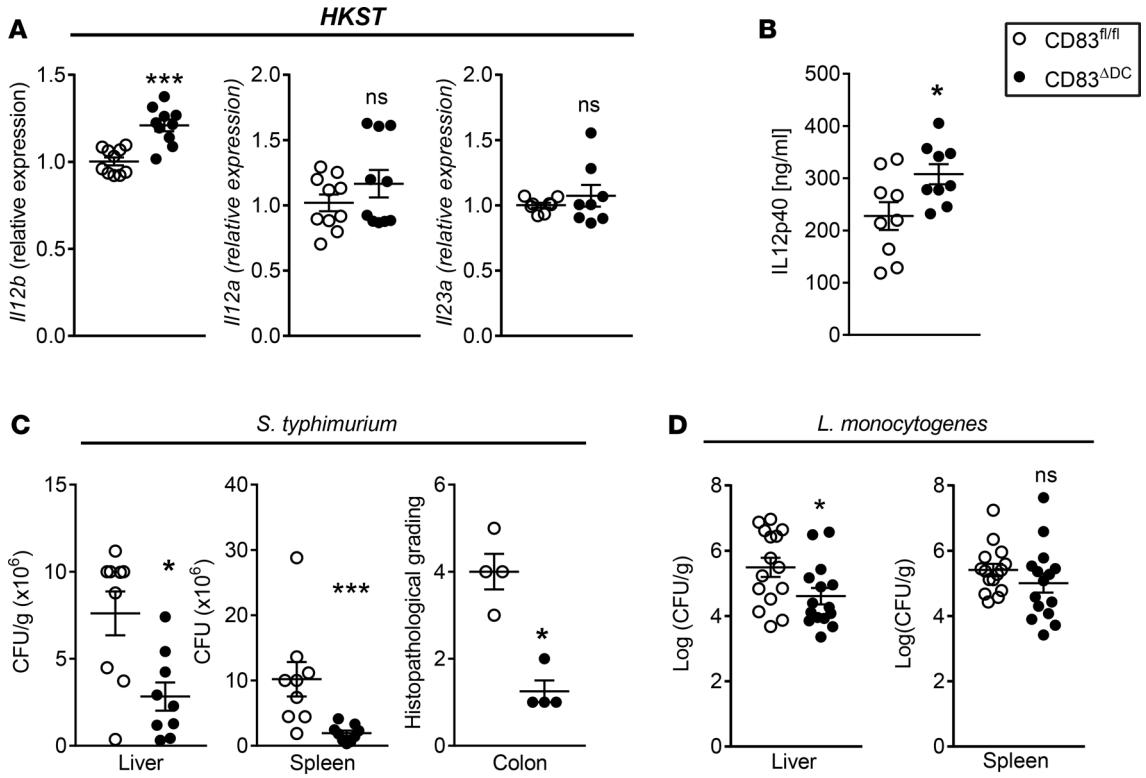

Figure 4. Lack of CD83 on DCs enhances immune responses against intracellular bacteria. (**A**) BMDCs from CD83$^{\Delta DC}$ or control mice were incubated with heat-killed *Salmonella tympimurium* (HKST) at a ratio of 10 bacteria per DC for 6 hours, and mRNA expression of *Il12a*, *Il12b*, and *Il23a* was assessed. Data are pooled from 3 independent experiments (n = 10). (**B**) Evaluation of IL-12p40 in the supernatants of BMDCs. Cells were stimulated with HKST at a ratio of 10 bacteria per DC for 16 hours, and supernatants were assessed by ELISA (n = 9, from 3 experiments). (**C**) Infection of CD83$^{\Delta DC}$ and control mice with *S. typhimurium* (n = 9; 1 representative experiment is shown). Mice were treated with 1.0 × 10^7 CFU intragastric (i.g.) and sacrificed 4 days later. (**D**) Infection of CD83$^{\Delta DC}$ and control mice with *L. monocytogenes*. Mice were infected intravenously with 1.0 × 10^4 CFU and were sacrificed 3 days later. Bacterial burden in liver and spleen was assessed by CFU counting of organ homogenates after 48 hours (n = 15, pooled from 3 independent experiments). Data are represented as mean ± SEM. Statistical analysis was performed using Mann-Whitney U test. *P < 0.05; ***P < 0.001; ns, not significant.

DC-specific CD83 deficiency leads to aggravated autoimmune neuroinflammation. Enhanced induction of immune responses is crucial for clearance of pathogens in acute infections but can be deleterious during chronic and autoimmune disorders. Additionally, we observed enhanced T cell stimulatory capacity of CD83-cKO DCs, associated with a Th17-favoring milieu. These data suggest induction of autoimmunity-prone T cell responses by CD83-deficient DCs. Therefore, we investigated how CD83 deficiency on DCs affects the control of immune responses to self-antigens in vivo. We used the $MOG_{35–55}$-induced EAE model, which is a well-established animal model for progressive CNS autoimmunity, leading to paralysis due to inflammation and demyelination-induced axonal damage (42). Mice were immunized with the $MOG_{35–55}$ peptide, and disease symptoms were monitored for up to 30 days. Interestingly, CD83$^{\Delta DC}$ mice succumbed more rapidly to the disease and showed a significantly impaired recovery phase, demonstrated by long-lasting and increased paralysis after the peak of disease, usually observed between days 15 and 18 (Figure 5A). The earlier onset of disease correlated with the infiltration of CD45$^+$ cells into the brain parenchyma (Figure 5B).

Breakdown of the blood-brain barrier and infiltration of peripheral immune cells into the CNS are hallmarks of EAE (43). To assess this process in more detail, we isolated cells from the brain and spinal cord of EAE mice at the peak of disease (day 15 after EAE induction) and determined the composition of CD45$^+$ leukocytes via flow cytometry. It is generally accepted that CNS-resident immune cells (i.e., microglial cells) can be segregated from infiltrating cells by their respective expression of CD11b and CD45 (44). While resident immune cells display CD11b, but only moderate levels of CD45, on their surface, infiltrating cells are CD45^{hi}, containing both CD11b$^-$ lymphoid and CD11b$^+$ myeloid cells (Figure 5C). At the peak of disease, CD83$^{\Delta DC}$ mice showed a markedly increased influx of peripheral immune cells, paralleled by a reduced proportion of resident cells (Figure 5D).

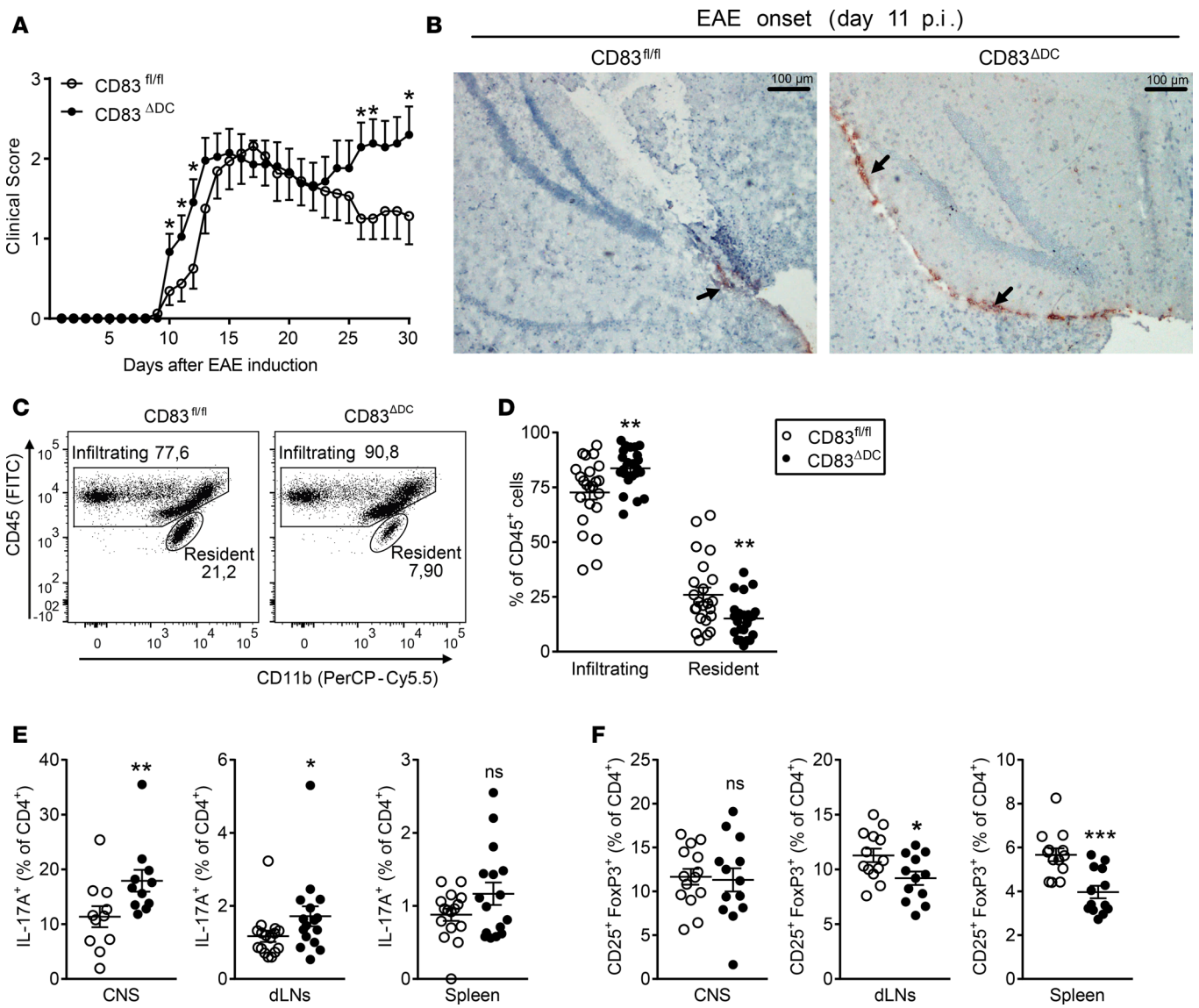

Figure 5. CD83 deficiency on DCs leads to exacerbated autoimmune neuroinflammation. (**A**) EAE was induced in 8- to 12-week-old female CD83$^{\Delta DC}$ or control mice by immunization with MOG_{35-55} peptide. Disease progression was monitored by scoring the level of paralysis for up to 30 days (CD83$^{fl/fl}$ n = 16, CD83$^{\Delta DC}$ n = 21; data are pooled from 3 independent experiments). (**B**) Histological analysis of infiltrating cells into the brain (black arrows). Mice were sacrificed on day 11 after EAE induction, and brain sections were obtained from frozen brains. Sections were stained with an anti-CD45 antibody (clone 104). One representative slide is shown for each group. (**C** and **D**) Assessment of CNS infiltration during EAE. At day 15 after EAE induction (peak of disease), total cells from brains and spinal cords were isolated and analyzed via flow cytometry. (**C**) Total CNS leukocytes (CD45$^+$ cells) were classified as resident or infiltrating cells, and (**D**) the respective proportion was analyzed (n = 16; data pooled from 4 independent experiments). (**E**) Analysis of IL-17 production in CD4$^+$ T cells from EAE animals. Single-cell suspensions from the CNS, draining inguinal lymph nodes (dLNs), or spleens, isolated from mice at EAE peak, were stimulated with PMA/ionomycin for 5 hours in the presence of Golgi transport inhibitors, and the intracellular amount of IL-17A was determined by flow cytometry (CNS n = 11; pooled from 3 experiments; dLNs/spleen n = 16; pooled from 4 experiments). (**F**) Assessment of regulatory T cell frequency in EAE mice. Single-cell suspensions from CNS, dLNs, or spleens, isolated from mice at EAE peak, were analyzed for the frequency of regulatory CD4$^+$ T cells (CD25$^+$FoxP3$^+$) (n = 13, pooled from 3 experiments). Data are represented as mean ± SEM. Statistical analysis was performed using Mann-Whitney U test. $^*P < 0.05$; $^{**}P < 0.01$; $^{***}P < 0.001$; ns, not significant.

During the EAE course, the CNS is infiltrated by IL-17–secreting CD4$^+$ T cells, and IL-17 further plays a crucial role in the induction and progression of the disease (45–47). Because we also observed preferential induction of Th17 responses by CD83-deficient DCs in vitro, we determined the presence of Th17 cells via the expression of IL-17 in CD4$^+$ T cells in different organs at the peak of disease. When analyzing the CNS of EAE animals, we detected a significantly enriched proportion of IL-17–producing CD4$^+$ T cells in CD83$^{\Delta DC}$ mice. Interestingly, elevated numbers of IL-17$^+$ cells were also present in draining inguinal lymph nodes of CD83$^{\Delta DC}$ mice at the peak of EAE, and we observed a similar trend for spleen-derived T cells of

those animals (Figure 5E and Supplemental Figure 4A). IFN-γ–producing $CD4^+$ and $CD8^+$ T cells revealed no difference between $CD83^{\Delta DC}$ and control mice (Supplemental Figure 4, B and C).

Because the recovery from EAE was significantly impaired in $CD83^{\Delta DC}$ mice and given the important role of Tregs for resolution of inflammation (48), we assessed whether this particular cell subset was affected in $CD83^{\Delta DC}$ mice. Infiltrating cells from the brain and spinal cord were isolated from EAE mice at the peak of disease, and the Treg frequency within the $CD4^+$ T cell compartment was analyzed. There were no overt differences in the percentages of $CD25^+FoxP3^+$ T cells between the CNS of $CD83^{\Delta DC}$ and control mice. However, when we analyzed the peripheral lymphoid organs, where disease priming is initiated, we observed a striking reduction of the Treg proportion in draining lymph nodes and spleens of $CD83^{\Delta DC}$ mice (Figure 5F). This effect was apparent only at the peak of disease, and Treg numbers in naive mice and during the initial disease phase (i.e., day 8 after EAE induction) were not significantly altered in $CD83^{\Delta DC}$ mice (Supplemental Figure 4, D and E). Thus, we demonstrate that CD83 deletion on DCs exaggerated development of chronic inflammatory processes paralleled by severely impaired regulatory mechanisms.

Discussion

Mature DCs that present self-antigens to autoreactive T cells are critically involved in the development of autoimmune diseases (2). This maturation process comprises upregulation of antigen-presenting MHC and costimulatory molecules as well as secretion of T cell–priming cytokines. One well-characterized marker for DC maturation is the CD83 protein. To unravel the physiological relevance of CD83 expression on DCs, we used a cKO system whereby CD83 expression was specifically deleted on both conventional DC subsets as well as BMDCs. These CD83-deficient DCs exhibited a reduced expression of MHC-II, which is in line with the previously described MARCH1-opposing effect of CD83 and subsequently higher ubiquitination and turnover of this protein (22).

Recent reports suggested that aberrant MHC-II expression disturbs DC homeostasis, which is hallmarked by decreased IL-12 production and T cell stimulatory capacity (37, 38). In contrast, CD83 deficiency, which enhances MHC-II degradation, resulted in increased IL-12 secretion by BMDCs upon challenge with HKST. Consequently, when infected with *S. typhimurium*, $CD83^{\Delta DC}$ mice revealed a strikingly reduced bacterial spreading to peripheral organs and ameliorated gut inflammation. Similar results were obtained upon infection with *L. monocytogenes*, with strongly reduced bacterial burdens in the liver of $CD83^{\Delta DC}$ mice. In summary, CD83 on DCs is an important modulator of protective responses against acute infections.

Because exaggerated immune responses are detrimental during chronic inflammatory processes, we investigated the impact of CD83 deletion on DCs using a well-established model for chronic and autoimmune neuroinflammation, the EAE. Thereby, we show that $CD83^{\Delta DC}$ mice succumb to disease more rapidly and display severely an impaired recovery with disturbed resolution of inflammation. This phenotype is characterized by increased inflammatory cell influx into the CNS and by elevated proportions of IL-17–producing T cells at the peak of disease. Because we also observed increased IL-17 secretion in DC–T cell cocultures, we propose that CD83-deficient DCs shape the microenvironment during initiation of the immune response in favor of a Th17 development.

Interestingly, during the course of EAE, $CD83^{\Delta DC}$ mice displayed reduced Treg numbers in peripheral immune organs but not in the CNS, despite a significantly impaired recovery phase. However, encephalitogenic CNS-infiltrating effector T cells are refractory to Treg-mediated suppression because of their unique proinflammatory cytokine profile (49). Additionally, the same study revealed that MOG-specific Tregs are not generated de novo but expand during EAE from preexisting natural Tregs. Because we observed reduced Treg numbers in the spleen and lymph nodes of $CD83^{\Delta DC}$ mice, with coincidently augmented Th17 proportions, we reason that $CD83^{\Delta DC}$ mice fail to induce a proper regulatory response in the periphery. Thus, these mice are unable to prevent the generation of further pathogenic T_{eff} cells and consequently exhibit impaired recovery from the autoimmune disease. Collectively, CD83 constitutes a new vital checkpoint that downregulates overshooting immune responses and induces resolution of inflammation.

Paralleled by the superior potential of $CD83^{\Delta DC}$ mice to mount proinflammatory immune responses in vivo, we observed an overactivated phenotype of CD83-deficient DCs in vitro. In contrast to decreased expression of MHC-II and CD86 due to lack of MARCH1 inhibition (22), CD83-cKO DCs displayed markedly elevated levels of CD25 and OX40L on their surface and produced more IL-2 in response to TLR-L activation. DC-derived IL-2 has been reported to bind to its high-affinity receptor, CD25, on DCs and is transpresented to T cells during antigen recognition, resulting in an enhanced early T cell activation (31).

In contrast, OX40L perpetuates T cell proliferation at later stages (50). Indeed, we observed augmented T cell proliferation upon coculture with antigen-loaded DCs derived from CD83$^{\Delta DC}$ animals. This suggests that elevated OX40L, CD25, and IL-2 expression may jointly compensate for probably compromised antigen-presenting capacity due to low MHC-II and CD86 expression. Noteworthily, the proliferative advantage of T cells activated by CD83-cKO DCs was abolished by blockade of OX40L, underlining the importance of this particular marker for induction of enhanced T cell proliferation. Interestingly, enforced expression of OX40L also aggravates the disease course in EAE mice, as seen in CD83$^{\Delta DC}$ animals (51).

Beyond initiation of T cell proliferation, quenching of IL-2 by DC-expressed CD25 has been shown to regulate T cell differentiation (52), and we noticed an increased propensity of CD83-deficient DCs to induce proinflammatory T cell responses in vitro. Thus, expression of IL-2 and CD25 could modulate the outcome of T cell priming by enforcing T effector differentiation.

In addition to a superior capacity to induce antigen-specific T cell proliferation, CD83-deficient DCs impair the suppressive capacity of Tregs. Because Tregs depend on IL-2 secretion by external sources, such as DCs (53), IL-2 quenching by CD83-cKO DCs might prevent expansion or induction of these regulatory cells. Interestingly, we indeed observed reduced proportions of Tregs in peripheral lymphoid organs in CD83$^{\Delta DC}$ mice during EAE but not in naive animals. These data suggest an impaired expansion or survival of Tregs derived from CD83$^{\Delta DC}$ mice during disease induction. However, we detected impaired suppressive function rather than defective Treg expansion in our in vitro culture system. It has been previously reported that Tregs display high levels of OX40 on their surface and enforced expression of OX40L on APCs or agonistic triggering of OX40 disrupts Treg suppressor functions and leads to reduced survival (54–56). Indeed, blocking of OX40L on the surface of CD83-deficient DCs reversed the enhanced T cell proliferation, which therefore may rely on mitigated Treg suppression by OX40–OX40L interaction. As a corollary, Treg survival might be impaired during immune responses in vivo.

The overactive phenotype observed in CD83-cKO DCs is also characterized by increased IRAK1 expression levels, which points toward an enhanced TLR signaling capacity. Interestingly, previous reports demonstrated that sCD83 also alters TLR signaling by binding to MD-2 on human monocytes, resulting in a long-lasting degradation of IRAK1 and subsequent induction of tolerogenic mechanisms (57). Likewise, CD83 on DCs could negatively modulate the TLR pathway either in *cis* or in *trans*, which would account for exaggerated inflammatory immune responses in CD83$^{\Delta DC}$ animals.

Previous in vitro studies suggested a costimulatory effect of CD83 on human DCs (26, 58) but no influence on the stimulatory capacity of murine APCs (28). Most of these reports focused on the initiation of antigen-specific T cell responses of both human and murine DCs lacking CD83 after maturation periods longer than 24 hours. However, DCs are primed by pathogens to produce IL-12, TNF-α, and IL-2 as early as 2 hours after stimulation (59, 60). Thus, secretion of activating and polarizing cytokines occurs shortly after activation, and assessment of in vitro stimulatory capacity at later time points may yield different results.

Here, we demonstrate that CD83-deficient BMDCs express elevated levels of IL-2 and IL-12 early (i.e., 6 hours) after stimulation and induce higher antigen-dependent T cell proliferation and a more proinflammatory milieu when cocultivated shortly after TLR activation. Thus, we suggest an important modulatory role of CD83 for DC homeostasis, similar to its impact on Tregs (25). Because aberrant expression of MHC-II disrupts normal DC function and CD83-deficient DCs display lower surface levels of MHC-II (37), this reduced expression may account for the increased proinflammatory phenotype of DCs derived from CD83$^{\Delta DC}$ mice.

In summary, we revealed that CD83 acts as a regulatory checkpoint module preventing overshooting immune responses, which eventually lead to autoimmunity. We provided evidence that DC-specific abrogation of CD83 results in intensified protective antibacterial immune responses but also aggravates autoimmune neuroinflammation. Deletion of CD83 confers a more proinflammatory phenotype on DCs, leading to potent induction of antigen-dependent T cell proliferation and Th17 commitment. Additionally, CD83-deficient DCs tend to subvert Treg suppressive capacity and thus impair the establishment of inflammation-resolving mechanisms. Finally, these findings may help find new pathways and therapeutic intervention strategies to specifically modulate DCs' functions in therapy for autoimmune disorders, such as multiple sclerosis, and in the prevention of bacterial infections.

Methods

Animals. All animals were maintained on a C57BL/6N background. $CD83^{fl/fl}$ mice were generated as described previously (29) and were crossed with *Itgax*-Cre mice for DC-specific depletion of the *Cd83* gene ($CD83^{\Delta DC}$). *Itgax*-Cre mice were provided by H.-M. Jäck (Department of Medicine 3, University Hospital Erlangen, Erlangen, Germany). G. Krönke (Department of Medicine 3, University Hospital Erlangen, Erlangen, Germany) provided tdTomato reporter animals. 2D2-transgenic mice were purchased from Jackson Laboratories.

For several experiments, we used *Itgax*-Cre mice, which harbor a WT CD83-encoding locus ($CD83wt^{Cre}$), as control animals to rule out the contribution of the Cre-recombinase to our results. In all tested in vitro and in vivo conditions, comparison of $CD83^{\Delta DC}$ animals to $CD83wt^{Cre}$ closely resembled results obtained with $CD83^{fl/fl}$ mice (Supplemental Figure 5).

EAE induction. Mice were immunized subcutaneously with 100 μL of emulsified complete Freund's adjuvant (MilliporeSigma) supplemented with 10 μg/μL *Mycobacterium tuberculosis* H37Ra (BD) and 100 μg $MOG_{35–55}$ peptide (Charité Berlin) and received intraperitoneal injections of 200 ng pertussis toxin (List Biological Laboratories) at the time of immunization and 48 hours later. Mice were monitored every other day for signs of clinical manifestation of EAE, and clinical scores were attributed as follows: 0, no disease; 1, tail weakness; 2, hind limb weakness; 3, hind limb paralysis; 4, hind limb paralysis with forelimb weakness; and 5, moribund or dead animals.

Infection with bacteria. For infection with *S. typhimurium*, mice were treated with 20 mg streptomycin i.g. 24 hours before i.g. infection with 1×10^7 CFU *S. typhimurium*. Bacterial counts were obtained by CFU plating assays using homogenates of the indicated organs on day 4 after infection.

Infection with *L. monocytogenes* 10403S was achieved by intravenous injection of 1.0×10^4 CFU per mice. For the determination of bacterial loads of liver and spleen, mice were killed after 3 days. The respective organs were isolated and homogenized in PBS. Serial dilutions of the homogenates were plated on Oxford agar plates and incubated at 37°C for 48 hours to allow CFU counting (61).

Generation and stimulation of BMDCs. For generation of BMDCs, both tibiae and femurs were flushed, and total BM cells were cultivated for 6–8 days in cell culture dishes in RPMI1640 medium (Lonza), supplemented with 10% FCS (Merck), 1% penicillin/streptomycin/L-glutamine solution (MilliporeSigma), and 0.5 μM β-mercaptoethanol (Roth) (R10 medium) and containing 10% supernatant of a GM-CSF–producing cell line (gift of M. Lutz, Institute for Virology and Immunobiology, University of Würzburg, Würzburg, Germany). Fresh medium and GM-CSF was added every 3 days. Loosely adherent and nonadherent cells were collected and transferred to 24-well plates (Thermo Fisher Scientific) for stimulations at densities of 0.5×10^6 to 1×10^6 cells per well. For mRNA and phenotype analyses, DCs were treated for 5 hours and 16 hours, respectively, with 0.5 μM CpG ODN2395 and 1 μg/mL Pam_3CSK_4 (Invivogen, Thermo Fisher Scientific). For coculture experiments, DCs were incubated with CpG OD2395 and Pam_3CSK_4 with 2 μg/mL $MOG_{35–55}$ peptide for 3 hours. Unstimulated $MOG_{35–55}$-loaded DCs served as negative controls. Stimulation with HKST was performed at a ratio of 10 bacteria per cell. Cytokine levels in supernatants of BMDCs were determined after 16 hours' stimulation either by cytometric bead array (BD and BioLegend) or ELISA (BioLegend) according to each manufacturer's instructions.

Immunohistochemistry. For visualization of inflammatory infiltrates, brains and spinal cords from mice (day 1 after EAE induction) were removed, placed in Tissue-Tek (Sakura) cryoprotective mold, fixed on dry ice, and stored at −80°C. Sections were sliced sequentially with a thickness of 5 μm with a cryotome (Kryocut CM 2000; Leica). Immunohistological staining was performed using an immunoperoxidase detection system in a wet chamber. Acetone-fixed sections were incubated in PBS. Endogenous peroxidase was blocked by incubating sections in 3% H_2O_2. The primary antibody was a biotinylated anti–mouse CD45.2 antibody (clone 104; Thermo Fisher Scientific). For detection and subsequent visualization, slides were treated with ABC and AEC Kits (Vector Laboratories), mounted in Aqua Tex (Roth), and covered with a coverslip.

Purification of nuclear and cytoplasmic protein fractions. Cell pellets were treated with cell lysis buffer (10 mM HEPES at pH 7.6, 0.1 mM EDTA, 10 mM KCl, 1 mM DTT, 5% glycerol, and 1× Protease Inhibitor Mix, Roche) and incubated 15 minutes on ice. Subsequently, 10% IGEPAL (MilliporeSigma) was added, and the cell membranes were disrupted by vortexing for 30 seconds. Cytoplasmic fraction was collected after a centrifugation step (2000 *g*, 5 minutes, 4°C). The residual nuclei pellet was washed twice in cell lysis buffer and resuspended in nuclear extraction buffer containing 20 mM HEPES at pH 7.6, 0.1 mM EDTA, 50 mM KCl, 1 mM DTT, 300 mM NaCl, 10% glycerol, and 1× Protease Inhibitor Mix (Roche). Afterward, nuclei were sonicated (40% amplitude, 45°C, 10 seconds,

5-minute pause), and the supernatant was collected after centrifugation (16000 *g*, 10 minutes, 4°C). Protein concentrations were determined via bicinchoninic acid assay according to the manufacturer's instructions (Thermo Fisher Scientific).

Western blot analyses. Nuclear and cytoplasmic lysates of stimulated BMDCs were denatured in reducing Laemmli buffer at 95°C for 5 minutes. After protein separation via polyacrylamide gel electrophoresis and blotting onto a nitrocellulose membrane (GE Healthcare), the membrane was blocked and subsequently probed with the following primary antibodies: mouse anti-NFATc2 (25A10.D6.D2, Invitrogen, Thermo Fisher Scientific), rabbit anti-Lamin A/C (2032S, Cell Signaling Technology), mouse anti-CD83 (F-5, Santa Cruz Biotechnology), rabbit anti-IRAK1 (D51G7, Cell Signaling Technology), or mouse anti–β-actin (AC-74, MilliporeSigma). These were diluted 1:1000 in 1× RotiBlock (Roth), added to the membranes, and incubated overnight at 4°C. Afterward, membranes were washed and the appropriate HRP-labeled secondary antibody (goat anti–rabbit IgG [catalog 7074] or horse anti–mouse IgG [catalog 7076], both from Cell Signaling Technology) was added. Signals on the blots were detected using ECL Prime Western Blotting Detection Reagent (GE Healthcare).

Isolation of 2D2 CD4$^+$ T cells and coculture with BMDCs. $MOG_{35–55}$-specific CD4$^+$ T cells were isolated from spleens and inguinal lymph nodes of 2D2 mice using either total or naive CD4$^+$ T cell isolation kits (Miltenyi Biotec). For proliferative analyses, T cells were labeled with CTV cell proliferation dye (Thermo Fisher Scientific) and cocultivated with MOG-loaded DCs at a T cell/DC ratio of 20:1 for 4 days. Proliferation was quantified using the median fluorescence intensity of CTV of the CD4$^+$ compartment. For the OX40L blocking experiments, 10 μg/mL of α-OX40L (RM134L) or isotype-matched control antibody (RTK4530) was added during the cultivation period (both BioLegend). Cytokine analyses were performed after 4 days of coculturing T cells and DCs at a ratio of 5:1 using a cytometric bead array according to the manufacturer's instructions (BioLegend).

For analysis of Treg suppressive capacity in DC cocultures, Tregs were isolated from spleens and inguinal lymph nodes of 2D2 mice using CD4$^+$CD25$^+$ Regulatory T Cell Isolation Kit, mouse (Miltenyi Biotec). CD25$^-$ T cells served as T_{eff} cells and were cocultivated with BMDCs stimulated as described above. T_{eff} cell/DC ratio was adjusted to 20:1, and Tregs were added at decreasing amounts. Suppressive capacity was calculated from division indices of Treg cocultures relative to T_{eff} cell/DC–only conditions.

Isolation of CNS-infiltrating cells. Immune cells within the CNS were isolated by a 1-step density centrifugation protocol as described previously (62), with modifications. Briefly, mice were perfused with ice-cold PBS by cardiac puncture, and brains were collected and placed in RPMI1640 medium without phenol red (Thermo Fisher Scientific) on ice. Tissue was homogenized with a tissue dounce grinder set (Kimble). Myelin was removed by centrifugation of homogenates resuspended with 37% Percoll (MilliporeSigma). Cells were collected in R10 medium and used either for restimulation and cytokine analysis or directly for flow cytometry. Resident CNS immune cells (i.e., microglia) were defined as CD11b$^+$CD45^{int}CX3CR1$^+$, whereas the CD45^{hi} population represented infiltrating lymphoid (CD11b$^-$) and myeloid (CD11b$^+$) cells.

Isolation and restimulation of cells. Spleens and draining inguinal lymph nodes were collected and ground between 2 microscope slides. Cells were passed through a 70-μm cell strainer Greiner Bio-One and washed with PBS. For spleens, lysis of erythrocytes was performed. Cells were collected in R10 medium for culture or used directly for flow cytometry. For intracellular staining of cytokines, cells were restimulated with 50 ng/mL PMA and 500 μg/mL ionomycin (MilliporeSigma) for 5 hours with Golgi transport inhibitors (Golgi-Plug and Golgi-Stop, BD) added for the last 4 hours.

Flow cytometry analysis. Surface staining was performed in PBS containing LIVE/DEAD Fixable Aqua Dead Cell Stain (Thermo Fisher Scientific) for 30 minutes at 4°C. For intracellular staining, cells were fixed and permeabilized, and intracellular staining was performed in Permeabilization Reagent (Thermo Fisher Scientific, 00-5523-00). Antibodies (all from BioLegend, unless otherwise stated) against the following antigens were used: CD3 (17A2), CD4 (RM4-5), CD8 (53-6.7), CD11b (M1/70), CD11c (N418), CD25 (PC61), CD45 (I3/2.3), CD83 (Michel19), CD86 (GL-1), FoxP3 (FJK-16s, eBioscience), IFN-γ (XMG1.2), IL-17A (TC11-18H10.1), I-A/I-E–FITC (2G9, BD), I-A/I-E (M5/114.152), and OX40L (RM134L). Expression was assessed using a FACSCantoII flow cytometer (BD) and analyzed with FlowJo software version 10 (FlowJo, LLC). Living leukocytes were gated for further analyses. To compensate for interassay variability, relative fluorescence intensities were calculated as a ratio of CD83$^{\Delta DC}$ to CD83$^{fl/fl}$.

Table 1. Primer sequences for qPCR

Gene	Orientation	Sequence
Cd83	Forward	5′-CGCAGCTCTCCTATGCAGTG-3′
	Reverse	5′-GTGTTTTGGATCGTCAGGGAATA-3′
Ido1	Forward	5′-ATTGGTGGAAATCGCAGCTTC-3′
	Reverse	5′-ACAAAGTCACGCATCCTCTTAAA-3′
Il12a	Forward	5′-AACAGGGTGATGGGCTATC-3′
	Reverse	5′-TGAGATGTGATGGGAGAACAG-3′
Il12b	Forward	5′-GGAAGCACGGCAGCAGAATAA-3′
	Reverse	5′-CTTGAGGGAGAAGTAGGAATG-3′
Il23a	Forward	5′-GCAACTTCACACCTCCCTAC -3′
	Reverse	5′-CGAAGGATCTTGGAACGGAG-3′
Il2	Forward	5′-AGCAGGATGGAGAATTACAGG-3′
	Reverse	5′-GTCAAATCCAGAACATGCCG-3′
Tgfb	Forward	5′-TGGAGCAACATGTGGAACTCTA-3′
	Reverse	5′-AGACAGCCACTCAGGCGTATC-3′
Rpl4	Forward	5′-GCTGAACCCTTACGCCAAGA-3′
	Reverse	5′-TCTCGGATTTGGTTGCCAGT-3′

qPCR. Cells were lysed with RLTPlus buffer (Qiagen) and stored at –80°C until RNA isolation. Total RNA was isolated using the RNeasy Plus Mini Kit (Qiagen), and mRNA was transcribed into cDNA using First Strand cDNA Synthesis Kit (Thermo Fisher Scientific). Gene expression was analyzed via qPCR and the SsoAdvanced Universal SYBR Green Supermix on a CFX96 Real-Time System (Bio-Rad) and normalized to the expression of the *Rpl4* reference gene. To compensate for interassay variability, relative expression levels were calculated as a ratio of $CD83^{\Delta DC}$ to $CD83^{fl/fl}$. All primers were designed and validated according to the Minimum Information for Publication of Quantitative Real-Time PCR Experiments guidelines. For primer sequences see Table 1.

Statistics. All statistics were performed with GraphPad Prism 7.0 using the Mann-Whitney *U* test for nonparametric data or 1-way ANOVA. Data are presented as mean values including the SEM. $*P < 0.05$; $**P < 0.01$; $***P < 0.001$; and $****P < 0.0001$ were considered statistically significant.

Study approval. Animal care and all experimental procedures of the present study were performed in accordance with the European Community Standards on the Care and Use of Laboratory Animals and were approved by our institutional ethics committee.

Author contributions

ABW designed, conducted, and analyzed the majority of experiments and prepared the manuscript. LK, KP, AB, CK, CS, LS, and EZ performed experiments, analyzed data, and edited the manuscript. JM, NG, MG, MP, and DS conducted the infection experiments with living bacteria and edited the manuscript. LN and THW provided scientific insight, supervised some analyses, and edited the manuscript. AS conceived and designed the study, supervised experiments, and prepared the manuscript.

Acknowledgments

This work was supported by the Deutsche Forschungsgemeinschaft (DFG) via the SFB1181 projects B03 (to AS), B06 (to LN), and C04 (to JM) and the Graduiertenkolleg 1660 grant B02 to AS. AS was further supported by the DFG project STE432/9-1, DS by the DFG project SO 1149/1-1, and JM by DFG grant MA 2621/4-1. KP was supported by the DFG Project ZI 1225/1-1.

Address correspondence to: Alexander Steinkasserer, Department of Immune Modulation, University Hospital Erlangen, Hartmann Street 14, 91052 Erlangen, Germany. Phone: 49.9131.853.6725; Email: alexander.steinkasserer@uk-erlangen.de.

1. Banchereau J, et al. Immunobiology of dendritic cells. *Annu Rev Immunol*. 2000;18:767–811.
2. Ganguly D, Haak S, Sisirak V, Reizis B. The role of dendritic cells in autoimmunity. *Nat Rev Immunol*. 2013;13(8):566–577.
3. Raker VK, Domogalla MP, Steinbrink K. Tolerogenic dendritic cells for regulatory T cell induction in man. *Front Immunol*. 2015;6:569.
4. Prazma CM, Tedder TF. Dendritic cell CD83: a therapeutic target or innocent bystander? *Immunol Lett*. 2008;115(1):1–8.
5. Zhou LJ, Schwarting R, Smith HM, Tedder TF. A novel cell-surface molecule expressed by human interdigitating reticulum cells, Langerhans cells, and activated lymphocytes is a new member of the Ig superfamily. *J Immunol*. 1992;149(2):735–742.
6. Cramer SO, Trumpfheller C, Mehlhoop U, Moré S, Fleischer B, von Bonin A. Activation-induced expression of murine CD83 on T cells and identification of a specific CD83 ligand on murine B cells. *Int Immunol*. 2000;12(9):1347–1351.
7. Breloer M, Fleischer B. CD83 regulates lymphocyte maturation, activation and homeostasis. *Trends Immunol*. 2008;29(4):186–194.
8. Kreiser S, et al. Murine CD83-positive T cells mediate suppressor functions in vitro and in vivo. *Immunobiology*. 2015;220(2):270–279.
9. von Rohrscheidt J, et al. Thymic CD4 T cell selection requires attenuation of March8-mediated MHCII turnover in cortical epithelial cells through CD83. *J Exp Med*. 2016;213(9):1685–1694.
10. Hock BD, Kato M, McKenzie JL, Hart DN. A soluble form of CD83 is released from activated dendritic cells and B lymphocytes, and is detectable in normal human sera. *Int Immunol*. 2001;13(7):959–967.
11. Hock BD, Haring LF, Steinkasserer A, Taylor KG, Patton WN, McKenzie JL. The soluble form of CD83 is present at elevated levels in a number of hematological malignancies. *Leuk Res*. 2004;28(3):237–241.
12. Hock BD, Fernyhough LJ, Gough SM, Steinkasserer A, Cox AG, McKenzie JL. Release and clinical significance of soluble CD83 in chronic lymphocytic leukemia. *Leuk Res*. 2009;33(8):1089–1095.
13. Packhäuser KRH, Roman-Sosa G, Ehrhardt J, Krüger D, Zygmunt M, Muzzio DO. A kinetic study of CD83 reveals an upregulation and higher production of sCD83 in lymphocytes from pregnant Mice. *Front Immunol*. 2017;8:486.
14. Zinser E, Lechmann M, Golka A, Lutz MB, Steinkasserer A. Prevention and treatment of experimental autoimmune encephalomyelitis by soluble CD83. *J Exp Med*. 2004;200(3):345–351.
15. Lan Z, et al. Prevention of chronic renal allograft rejection by soluble CD83. *Transplantation*. 2010;90(12):1278–1285.
16. Ge W, et al. Immunosuppression involving soluble CD83 induces tolerogenic dendritic cells that prevent cardiac allograft rejection. *Transplantation*. 2010;90(11):1145–1156.
17. Eckhardt J, et al. Soluble CD83 ameliorates experimental colitis in mice. *Mucosal Immunol*. 2014;7(4):1006–1018.
18. Royzman D, et al. Soluble CD83 triggers resolution of arthritis and sustained inflammation control in IDO dependent manner. *Front Immunol*. 2019;10:633.
19. Lan Z, et al. Induction of kidney allograft tolerance by soluble CD83 associated with prevalence of tolerogenic dendritic cells and indoleamine 2,3-dioxygenase. *Transplantation*. 2010;90(12):1286–1293.
20. Bock F, et al. Topical application of soluble CD83 induces IDO-mediated immune modulation, increases Foxp3+ T cells, and prolongs allogeneic corneal graft survival. *J Immunol*. 2013;191(4):1965–1975.
21. Kuwano Y, et al. CD83 influences cell-surface MHC class II expression on B cells and other antigen-presenting cells. *Int Immunol*. 2007;19(8):977–992.
22. Tze LE, et al. CD83 increases MHC II and CD86 on dendritic cells by opposing IL-10-driven MARCH1-mediated ubiquitination and degradation. *J Exp Med*. 2011;208(1):149–165.
23. Liu H, et al. Ubiquitin ligase MARCH 8 cooperates with CD83 to control surface MHC II expression in thymic epithelium and CD4 T cell selection. *J Exp Med*. 2016;213(9):1695–1703.
24. Fujimoto Y, et al. CD83 expression influences CD4+ T cell development in the thymus. *Cell*. 2002;108(6):755–767.
25. Doebbeler M, et al. CD83 expression is essential for Treg cell differentiation and stability. *JCI Insight*. 2018;3(11):99712.
26. Prechtel AT, Turza NM, Theodoridis AA, Steinkasserer A. CD83 knockdown in monocyte-derived dendritic cells by small interfering RNA leads to a diminished T cell stimulation. *J Immunol*. 2007;178(9):5454–5464.
27. Pinho MP, Migliori IK, Flatow EA, Barbuto JA. Dendritic cell membrane CD83 enhances immune responses by boosting intracellular calcium release in T lymphocytes. *J Leukoc Biol*. 2014;95(5):755–762.
28. Kretschmer B, et al. CD83 on murine APC does not function as a costimulatory receptor for T cells. *Immunol Lett*. 2008;120(1-2):87–95.
29. Krzyzak L, et al. CD83 Modulates B cell activation and germinal center responses. *J Immunol*. 2016;196(9):3581–3594.
30. Bates JM, et al. Dendritic cell CD83 homotypic interactions regulate inflammation and promote mucosal homeostasis. *Mucosal Immunol*. 2015;8(2):414–428.
31. Wuest SC, et al. A role for interleukin-2 trans-presentation in dendritic cell-mediated T cell activation in humans, as revealed by daclizumab therapy. *Nat Med*. 2011;17(5):604–609.
32. Khameneh HJ, Ho AW, Spreafico R, Derks H, Quek HQ, Mortellaro A. The Syk-NFAT-IL-2 pathway in dendritic cells is required for optimal sterile immunity elicited by alum adjuvants. *J Immunol*. 2017;198(1):196–204.
33. Ito T, et al. OX40 ligand shuts down IL-10-producing regulatory T cells. *Proc Natl Acad Sci U S A*. 2006;103(35):13138–13143.
34. Liang D, et al. Role of CD25+ dendritic cells in the generation of Th17 autoreactive T cells in autoimmune experimental uveitis. *J Immunol*. 2012;188(11):5785–5791.
35. Kadowaki N. Dendritic cells: a conductor of T cell differentiation. *Allergol Int*. 2007;56(3):193–199.
36. Zhang Y, et al. TNF-α promotes early atherosclerosis by increasing transcytosis of LDL across endothelial cells: crosstalk between NF-κB and PPAR-γ. *J Mol Cell Cardiol*. 2014;72:85–94.
37. Ohmura-Hoshino M, et al. Cutting edge: requirement of MARCH-I-mediated MHC II ubiquitination for the maintenance of conventional dendritic cells. *J Immunol*. 2009;183(11):6893–6897.
38. Ishikawa R, Kajikawa M, Ishido S. Loss of MHC II ubiquitination inhibits the activation and differentiation of CD4 T cells. *Int Immunol*. 2014;26(5):283–289.
39. Godinez I, Keestra AM, Spees A, Bäumler AJ. The IL-23 axis in Salmonella gastroenteritis. *Cell Microbiol*. 2011;13(11):1639–1647.
40. Gilchrist JJ, MacLennan CA, Hill AV. Genetic susceptibility to invasive Salmonella disease. *Nat Rev Immunol*. 2015;15(7):452–463.
41. Berberich C, Ramírez-Pineda JR, Hambrecht C, Alber G, Skeiky YA, Moll H. Dendritic cell (DC)-based protection against an intracellular pathogen is dependent upon DC-derived IL-12 and can be induced by molecularly defined antigens. *J Immunol*.

2003;170(6):3171–3179.
42. Berard JL, Wolak K, Fournier S, David S. Characterization of relapsing-remitting and chronic forms of experimental autoimmune encephalomyelitis in C57BL/6 mice. *Glia*. 2010;58(4):434–445.
43. Ouyang S, Hsuchou H, Kastin AJ, Mishra PK, Wang Y, Pan W. Leukocyte infiltration into spinal cord of EAE mice is attenuated by removal of endothelial leptin signaling. *Brain Behav Immun*. 2014;40:61–73.
44. Casella G, et al. IL-27, but not IL-35, inhibits neuroinflammation through modulating GM-CSF expression. *Sci Rep*. 2017;7(1):16547.
45. Komiyama Y, et al. IL-17 plays an important role in the development of experimental autoimmune encephalomyelitis. *J Immunol*. 2006;177(1):566–573.
46. Han L, Yang J, Wang X, Li D, Lv L, Li B. Th17 cells in autoimmune diseases. *Front Med*. 2015;9(1):10–19.
47. McGinley AM, Edwards SC, Raverdeau M, Mills KHG. Th17 cells, γδ T cells and their interplay in EAE and multiple sclerosis. *J Autoimmun*. 2018:87:97–108.
48. O'Connor RA, Malpass KH, Anderton SM. The inflamed central nervous system drives the activation and rapid proliferation of Foxp3+ regulatory T cells. *J Immunol*. 2007;179(2):958–966.
49. Korn T, et al. Myelin-specific regulatory T cells accumulate in the CNS but fail to control autoimmune inflammation. *Nat Med*. 2007;13(4):423–431.
50. Rogers PR, Song J, Gramaglia I, Killeen N, Croft M. OX40 promotes Bcl-xL and Bcl-2 expression and is essential for long-term survival of CD4 T cells. *Immunity*. 2001;15(3):445–455.
51. Ndhlovu LC, Ishii N, Murata K, Sato T, Sugamura K. Critical involvement of OX40 ligand signals in the T cell priming events during experimental autoimmune encephalomyelitis. *J Immunol*. 2001;167(5):2991–2999.
52. Li J, Lu E, Yi T, Cyster JG. EBI2 augments Tfh cell fate by promoting interaction with IL-2-quenching dendritic cells. *Nature*. 2016;533(7601):110–114.
53. Kulhankova K, Rouse T, Nasr ME, Field EH. Dendritic cells control CD4+CD25+ Treg cell suppressor function in vitro through juxtacrine delivery of IL-2. *PLoS ONE*. 2012;7(9):e43609.
54. Valzasina B, Guiducci C, Dislich H, Killeen N, Weinberg AD, Colombo MP. Triggering of OX40 (CD134) on CD4(+)CD25+ T cells blocks their inhibitory activity: a novel regulatory role for OX40 and its comparison with GITR. *Blood*. 2005;105(7):2845–2851.
55. Vu MD, et al. OX40 costimulation turns off Foxp3+ Tregs. *Blood*. 2007;110(7):2501–2510.
56. Zhang X, et al. OX40 costimulation inhibits Foxp3 expression and Treg induction via BATF3-dependent and independent mechanisms. *Cell Rep*. 2018;24(3):607–618.
57. Horvatinovich JM, et al. Soluble CD83 inhibits T cell activation by binding to the TLR4/MD-2 complex on $CD14^+$ monocytes. *J Immunol*. 2017;198(6):2286–2301.
58. Aerts-Toegaert C, et al. CD83 expression on dendritic cells and T cells: correlation with effective immune responses. *Eur J Immunol*. 2007;37(3):686–695.
59. Yrlid U, Wick MJ. Antigen presentation capacity and cytokine production by murine splenic dendritic cell subsets upon Salmonella encounter. *J Immunol*. 2002;169(1):108–116.
60. Granucci F, Feau S, Angeli V, Trottein F, Ricciardi-Castagnoli P. Early IL-2 production by mouse dendritic cells is the result of microbial-induced priming. *J Immunol*. 2003;170(10):5075–5081.
61. Kastner R, et al. LipA, a tyrosine and lipid phosphatase involved in the virulence of Listeria monocytogenes. *Infect Immun*. 2011;79(6):2489–2498.
62. Legroux L, Pittet CL, Beauseigle D, Deblois G, Prat A, Arbour N. An optimized method to process mouse CNS to simultaneously analyze neural cells and leukocytes by flow cytometry. *J Neurosci Methods*. 2015;247:23–31.